Compact fiber-ring resonator for blue external cavity diode laser stabilization

Georges Perin, Dominique Mammez, Antoine Congar, Pascal Besnard, Karim Manamanni, Vincent Roncin, Frédéric Du Burck, Stéphane Trebaol

Research Article | Vol. 29, No. 23 / 8 Nov 2021 / Optics Express 37200
Optics EXPRESS

Compact fiber-ring resonator for blue external cavity diode laser stabilization

GEORGES PERIN,[1] DOMINIQUE MAMMEZ,[1] ANTOINE CONGAR,[1] PASCAL BESNARD,[1] KARIM MANAMANNI,[2] VINCENT RONCIN,[2] FRÉDÉRIC DU BURCK,[2] AND STÉPHANE TREBAOL[1,*]

[1] *Univ Rennes, CNRS, Institut FOTON - UMR 6082, F- 22305 Lannion, France*
[2] *Laboratoire de Physique des Lasers UMR CNRS 7538, Université Sorbonne Paris Nord Paris 13, 93430 Villetaneuse, France*
[*] *stephane.trebaol@enssat.fr*

Abstract: We demonstrate a compact and low-cost all-fiber-based locking setup for frequency-noise suppression of a 420 nm external-cavity diode laser. Frequency noise reduction in the 100 Hz to 800 kHz range is demonstrated up to 40 dB associated with a linewidth narrowing from 850 kHz to 20 kHz for 10 ms integration time. This simple locking scheme might be implemented for a large range of wavelengths and can be integrated on a small footprint for embedded applications requiring narrow linewidth blue laser diodes.

1. Introduction

Blue laser diodes (405-460 nm) are used in a large variety of applications ranging from lightening to wireless [1] or underwater [2,3] optical communications. These sources may also have many applications for gas sensing [4,5] atomic clocks [6], laser cooling [7–9] and pumping of alkali-metal-based 4-level active optical clocks as Cesium or Rubidium [10,11]. However, precision laser spectroscopy applications are demanding in term of laser performances [12–16]. In particular narrow linewidth, high stability, large output optical power and low power consumption are requested. Moreover, those needs are more and more associated with the quest for compactness to fit with lab-to-market technology transfer. In the infrared (IR) part of the spectrum, the laser diode technology is mature to address those kind of specifications [17] but for shorter wavelengths there are still technological issues. Currently, commercial blue laser diodes based on gallium nitride (GaN) have a wide multimode optical spectrum. Recently, demonstrations of DFB-like GaN laser diode have been reported [18–20] paving the way towards fully integrated devices. Indeed their compactness, efficiency and therefore power consumption make them more interesting devices than frequency-doubled lasers, which suffer from low conversion efficiency. To improve the frequency noise performances of laser diodes, the use of an external cavity (external cavity diode laser, ECDL) has been proven [12–16,21] to favor single mode behavior and, depending on the cavity finesse, it enables the natural laser-linewidth to be reduced. Nevertheless, opto-mechanical instabilities of the external cavity generate various low frequency noises, which limit the laser linewidth to a few MHz for integration times on the order of tens of ms. Various methods were developed in the near- (NIR) and mid- (MIR) infrared for laser stabilization in order to reduce the frequency-noise (FN) and achieve narrow and stable linewidths. The common feature of these methods is the use of a low-noise frequency reference, which can take various form depending on the level of stability to be reached. Reference based on molecular or atomic absorption lines enable laser linewidths of a few kHz over tens of seconds [22–24]. There also exists optical references independent from the laser wavelength like interferometers [25–27] or fiber-ring cavities [28–30] to provide mid-term stabilization over a few seconds. Nevertheless, the complexity of implemented servolocking schemes implies the use of fibered optical elements like acousto-optics modulators, isolators or attenuators, which are either not available nor provide

#435513 https://doi.org/10.1364/OE.435513
Journal © 2021 Received 20 Jul 2021; revised 23 Sep 2021; accepted 27 Sep 2021; published 26 Oct 2021

Optics EXPRESS

good performances at blue wavelengths. Thus, those techniques are not directly transferable to the blue range. Until now and to our knowledge, only atomic spectroscopy-based techniques were applied in the blue-violet range [31,32] to stabilize the emission wavelength at long time scale (up to 1 second average). In this paper, we present a versatile and compact optical reference based on an all-fiber-ring resonator to reduce short term frequency fluctuations, up the µs range, of a GaN based laser emitting in the blue range. The noise reduction performances are demonstrated on an ECDL laser by analyzing its frequency noise. In the following, section 2 describes the experimental setup for frequency noise reduction and in particular the fiber-ring resonator optical reference, the frequency noise measurement bench and the servolocking scheme. Section 3 aims to model the locking scheme performances. In section 4, we report on the frequency noise reduction performances of the system by comparing the experimental results to the simulations, which enables us to identify the origin of the noise reduction limitation.

2. Experimental setup for frequency noise reduction

2.1. Fiber-ring frequency reference

The schematic of the experimental setup is depicted in Fig. 1. The optical fiber ring, used as a frequency reference, is composed of a 2 m-long single-mode optical fiber spliced to a 60/40 coupler (60 % transmission and with 2.75 dB of optical losses). Those parameters are chosen to reach critical coupling regime to optimize the locking performances. The laser to lock is an ECDL emitting 40 mW at a wavelength of 420 nm. The laser frequency is modulated over a few GHz, by applying a saw tooth modulation on the current controller, to scan the transfer function of the optical cavity. The output cavity signal is collected by a fast photodiode with a DC-200 MHz bandwidth. Figure 2 displays the normalized optical cavity transfer function (blue curve). The transmission at resonance T_{min} drops down to 0.03, the free spectral range is closed to 103 MHz and the full-width at half maximum (FWHM) reaches 20 MHz. This leads to a quality factor Q of 3×10^7 at 420 nm. To reduce environmental acoustic and thermal perturbations, the fiber ring is sandwiched between two slices of foam (40x100x20 mm). The optical reference is then inserted and covered in a cardboard box (100x150x210 mm) with walls covered by anechoic shaped foam.

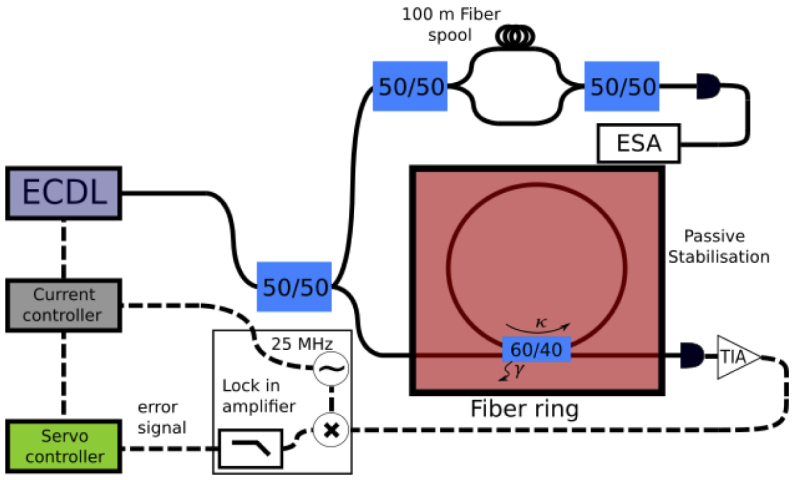

Fig. 1. Experimental setup for the locking of an ECDL on a 2 m passively stabilized fiber ring. The 60/40 coupler is characterized by a transmission coefficient $\kappa = 60\%$ and optical losses $\gamma = 2.75$ dB. The 420 nm single mode fiber used for the cavity is a non-polarisation maintaining fiber (non-PM) from NUFERN.

Optics EXPRESS

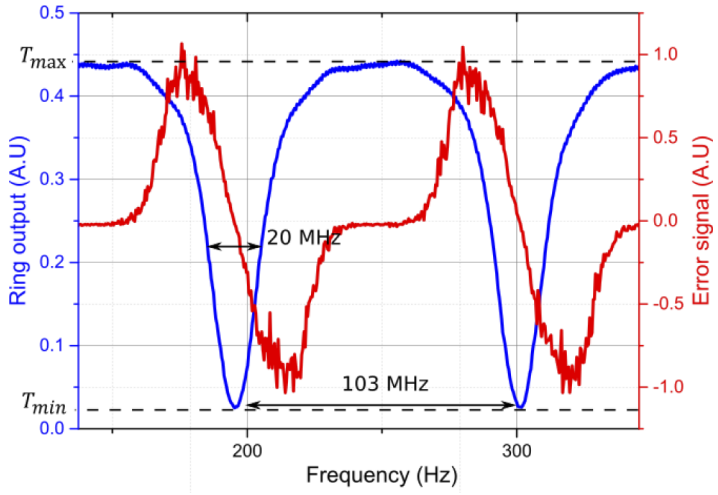

Fig. 2. Normalized transmission of the fiber ring cavity (blue curve) and normalized error signal at the output of the locking amplifier (red curve).

2.2. Frequency noise measurement

To evaluate the locking scheme performances, the frequency noise of the ECDL is characterized using a correlated delayed self-homodyne measurement setup composed of an unbalanced fiber-based Mach-Zehnder interferometer [33] enabling to characterize the laser frequency noise power spectral density between DC and 1.3 MHz with a noise floor level below 100 Hz^2/Hz in this configuration. The noise floor is mainly determined by the laser intensity noise, captured by the measurement bench, which is at least 25 dB below measured laser frequency noises. The free-running frequency noise (FN) of the ECDL is presented in Fig. 4 (red curve). The ECDL FN displays the usual behavior of such a laser with a 1/f slope at low frequency (below 100 kHz) followed, at higher frequency, by a white frequency noise-like contribution. This FN can be modeled by the expression $S_{\Delta\nu}(f) = h_{-1}/f + h_0$, with $h_{-1} = 144 \times 10^9$ Hz^3/Hz and $h_0 = 40 \times 10^3$ Hz^2/Hz. The free running laser parameters are extracted experimentally. For the free running laser, the intrinsic linewidth is then deduced from $\Delta\nu = \pi \times h_0$, which gives 126 kHz. The integrated linewidth can be estimated using the beta-line approach [34]. For an integration time of 10 ms, the free running laser integrated linewidth reaches 850 $\pm$ 146 kHz.

2.3. Servolocking scheme

To reduce the laser frequency noise, the ECDL laser frequency has to be locked on the transmission minimum of a cavity resonance. To do so, a Pound-Drever-Hall (PDH) [35] technique is implemented as shown in Fig. 1. The laser frequency modulation is obtained by direct modulation of the current controller driven by a RF signal generated by the lock-in amplifier. The signal at the output of the ring is detected and amplified by a transimpedance photodetector subsequently mixed with the RF signal and then filtered by the lock-in. The resulting error signal is plotted on Fig. 2 (red curve). Its shape corresponds to the derivative of the transfer function of the cavity (blue curve) as expected for such an open-loop configuration. Then, the error signal is sent to the servo controller box (see Fig. 1), which is a PI (Proportional Integral) card, to produce a correction signal sent to the current controller for laser frequency correction. In this work, the PDH technique is implemented using a 25 MHz modulation frequency, which is of the same order as the fiber ring linewidth (20 MHz). Indeed, we do not observe side bands as it is usual for PDH error signals. To evaluate the degradation of the error signal slope versus the modulation

Optics EXPRESS

frequency we run simulations using the model of the optoelectronic feedback loop described in section 3. The error signal slope variation is of the order of 8% for modulation ranging from 25 MHz to 50 MHz confirming that no high speed modulation is needed in our configuration.

The ECDL is then locked onto a fiber ring resonance thanks to the generated error signal. The resulting frequency noise of the locked laser is presented in Fig. 4 (blue curve). From 100 Hz to 1 kHz the FN level continuously decreases to reach 5×10^3 Hz^2/Hz, corresponding to a noise reduction in respect to the free running laser of more than 30 dB at 1 kHz. The locked laser FN displays a constant level between 1 kHz to 300 kHz. This behavior demonstrates the relative stability of the ring cavity compare to the ECDL laser. The noise level increases progressively above 300 kHz to reach the free running FN at 800 kHz corresponding to the upper limit of the locking bandwidth for which, the accumulated phase in the servoloop reaches 180°. Using the betaline estimation, the laser linewidth integrated over 10 ms is reduced from 850 kHz ± 146 kHz, for the laser in free running regime, to 20 ± 3 kHz for the locked laser, which corresponds to a reduction factor of 40 demonstrating that even a simple locking architecture can offer interesting performances in terms of FN and linewidth reductions. To identify the limiting contribution to the measured FN, we propose a model of the servolocking architecture in the next section.

3. Performance model of the locking scheme

The model developed in this section aims to identify the limiting contribution to the FN of the locked laser. In particular, we address the contribution of the Q-factor and coupling regime of the ring cavity as potential candidate to explain the overall behavior of the measured FN.

The block diagram of the experimental setup is described on Fig. 3. The input variable of the servoloop is the central frequency ν_{ref} of one of the ring resonances. The output of the close loop ν_{lock} is compared to the reference frequency ν_{ref} to produce a frequency difference. The frequency difference is converted into a voltage error signal ϵ through the frequency discriminator, represented by K_2 (an expression of K_2 can be found in Eq. 18) in the appendix), which results from the combination effects of the ring resonance, the photodiode, the transimpedance gain and the demodulation of the lock-in amplifier. The error signal ϵ is then converted into the correction signal S_{corr} through the PI corrector coefficients. Finally, the signal is converted back into a frequency correction signal through the actuator corresponding to the current driver represented by K_1. The frequency of the free running laser $S_{\nu_{\mathrm{ECDL}}}$ is then added at the actuator output summing point. The laser frequency is considered as a perturbation of the servoloop. The discriminator noise N_{dis}, corresponding to the shot noise is added by the photodetection process.

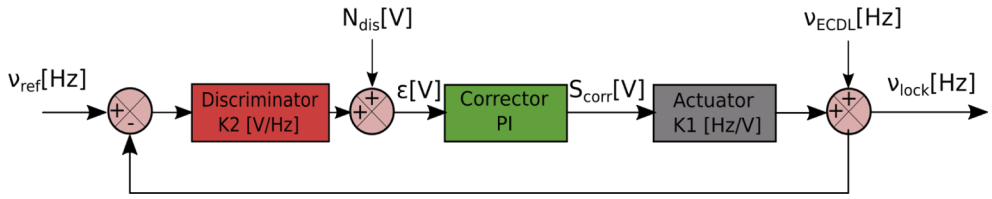

Fig. 3. Close loop block diagram of the ECDL locked on the optical fiber ring resonance (ν_{ref}). Various noise contributions are considered as the noise of the discriminator (N_{dis}) and the FN noise (ν_{ECDL}). ν_{lock} corresponds to the FN of the locked laser.

We can then express the open loop transfer function by:

$$G_{OL}(\omega) = K_2 C(\omega) K_1(\omega) \tag{1}$$

with C, the transfer function of the corrector described by:

$$C(\omega) = g * (P + \frac{1}{Ij\omega}) \tag{2}$$

Optics EXPRESS

where g is the gain of the corrector with a maximum value of 26 dB, and P and I the proportional and integral parameters respectively. Those values are chosen to reach a 1 MHz-correction bandwidth. Finally, the K_1 coefficient (in Hz/V) describing the actuator is experimentally evaluated by using a swept sine method [36].

To evaluate the performances of the close loop, in particular to determine the ability of the stabilization scheme to reduce the frequency noise of the laser, we observe the closed loop transfer function. As we manipulate random signals, we need to consider the power spectral density (expressed in Hz^2/Hz):

$$S_{lock} = \left|\frac{G_{OL}}{1+G_{OL}}\right|^2 S_{\nu_{ref}} + \left|\frac{G_{OL}}{1+G_{OL}}\right|^2 \left|\frac{1}{K2}\right|^2 S_{N_{dis}} + \left|\frac{1}{1+G_{OL}}\right|^2 S_{\nu_{\mathrm{ECDL}}} \tag{3}$$

The frequency noise of the laser is composed of three noise contributions. The first one is associated with the noise of the fiber ring cavity, the second term is linked to the noise of the discriminator, and finally the last term is related to the frequency noise of the free running laser. In the following, we will study the contribution of those three terms. In a first approximation, we consider the fiber ring frequency noise, $S_{\nu_{ref}}$ as a negligible contribution to the locked laser FN, which implies $S_{\nu_{\mathrm{ECDL}}} \gg S_{\nu_{ref}}$. This seems to be a reasonable assumption since we experimentally observe a drastic reduction of the FN of the laser when locked to the fiber ring. Omitting the discriminator contribution N_{dis}, Eq. (3) reduces to :

$$S_{lock} = \left|\frac{1}{1+G_{OL}}\right|^2 S_{\nu_{ECDL}} \tag{4}$$

From Eq. (4), we plot on Fig. 4 the expected locked laser FN (purple curve) feeding the model from experimentally determined coefficients of the open loop gain (Eq. (1)) and the measured free

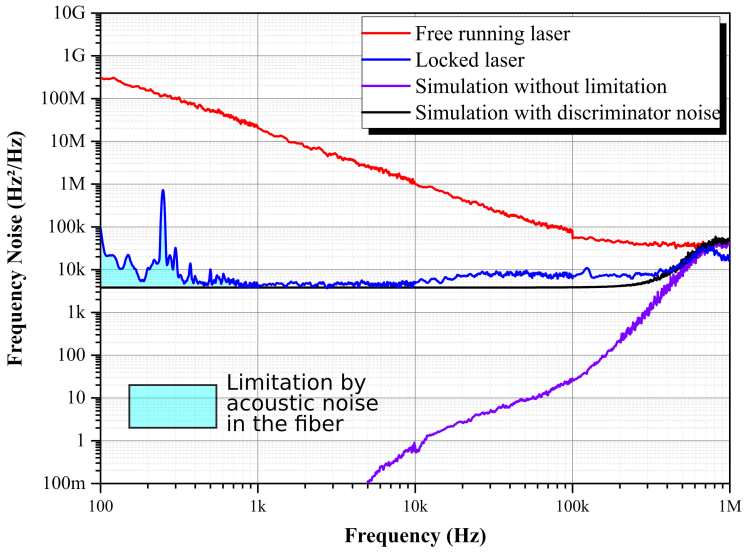

Fig. 4. Comparison between frequency noise of the free running laser (red curve), the locked laser (blue curve), the simulation without limitation (purple curve, Eq. (4)), and the simulation with the discriminator noise contribution (black curve, Eq. (5)). Frequency noise measurements have been averaged over 300 spectra.

Optics EXPRESS

running FN $S_{\nu_{\mathrm{ECDL}}}$ (red curve). We observe a clear discrepancy between the measured FN of the locked laser and the modeled FN without considering any limitations. This difference between simulated and measured locked laser FN indicates that other noise sources might contribute to the observed performances. In the following, we discuss the contribution of those noise sources.

4. Results and limitations

We focus on the performances limitations related to the Q-factor of the fiber-ring cavity. As we mentioned previously, the fiber ring acts as a frequency discriminator and then converts frequency variations into amplitude variations that are subsequently detected by the photodiode. To be able to detect the laser frequency noise, the slope of the error signal has to be sufficiently sharp to generate a corresponding intensity noise level larger than the shot noise level of the photodiode. This corresponds to the noise N_{dis} added after the discriminator on the block diagram of Fig. 3. The expression of the locked laser FN becomes:

$$S_{lock} = \left|\frac{G_{OL}}{1+G_{OL}}\right|^2 S_Q + \left|\frac{1}{1+G_{OL}}\right|^2 S_{\nu_{ECDL}} \tag{5}$$

where S_Q represents the equivalent noise in $\mathrm{Hz}^2/\mathrm{Hz}$ of the discriminator. The complete derivation of S_Q from the cavity and PDH parameters is given in the appendix and rise to :

$$S_Q \approx \left|\frac{1}{K2}\right|^2 S_{N_{dis}} = \frac{q\Delta\nu^2}{87\ SP}\left[\frac{1}{T_{max}J_1^2} + \frac{2}{T_{min}J_0^2}\right] \tag{6}$$

with $S_{N_{dis}}$ the power spectral density of the shot noise taken after the lock-in amplifier, q the elementary electrical charge, $\Delta\nu$ the width of a resonance, S the photodiode sensitivity, P the power at the input of the fiber ring, T_{min} the cavity minimum transmission, T_{max} the cavity maximum transmission and J_i the Bessel function taken at the modulation index.

On Fig. 4, we plot the S_Q white frequency noise (black curve). All the parameters introduced in the model are experimentally evaluated. The simulated curve is superimposed to the measured locked laser FN (blue curve) above 1 kHz showing that the S_Q contribution is limiting the frequency noise reduction of this locking scheme (black curve). In the following we propose to draw the origins of this limitation.

Firstly, we can underline the fact that the closed loop has no regulation effects on the white noise contribution introduced by S_Q. Indeed, as expressed in Eq. (5), the open loop gain G_{OL} is much larger than 1, which reduces $\left|\frac{G_{OL}}{1+G_{OL}}\right|^2$ to 1. This noise contribution should then be as low as possible to optimize the locked laser FN.

Secondly, the design of the cavity has to be optimized to reduce the discriminator noise contribution S_Q (see Eq. (6)). In particular the $\Delta\nu^2$ dependency of S_Q suggests that the resonance linewidth has to be as small as possible meaning that a large cavity Q-factor is need. Nevertheless, fiber ring resonator Q-factor at short wavelengths is bounded by (i) the attenuation loss in single mode optical fibers (> 30 dB/km @ 420 nm) and (ii) the coupler losses γ (2.75 dB). Those main limitations should be overcome by further improvements of fiber based optical elements performances at short wavelengths allowing to further reduce this FN limitation. Introducing the experimentally evaluated parameter values in Eq. (6) we obtain an estimation of S_Q equal to $4074 \pm 1267\ \mathrm{Hz}^2/\mathrm{Hz}$.

The S_Q limitation can usually be omitted in state-of-the-art frequency locking scheme at infrared wavelengths since fiber ring cavity Q-factor can rise up to 10^9 [37], which leads to an estimated S_Q of $0.1\ \mathrm{Hz}^2/\mathrm{Hz}$ corresponding sub-Hz intrinsic linewidth.

Below 1 kHz, locked laser FN is not anymore superimposed to the simulated S_Q curve. This low-frequency noise contribution might be related to acoustic noise captured by the fiber either

Optics EXPRESS

through the fiber ring or the homodyne bench acting as an efficient environmental sensor [25,26]. To reduce this noise input, long-term stabilization on a molecular transition can be coupled to the present frequency noise scheme to extend the FN noise reduction below 1 kHz [32].

5. Conclusion

We demonstrate, with a simple opto-electronic loop, a large frequency noise reduction using an all-optical fiber ring as a frequency reference. The performances of the locking scheme are demonstrated on an external cavity diode laser emitting at 420 nm. We achieve a noise reduction up to 40 dB below 1 kHz and a reduction of the laser linewidth up to a factor of 40. Simulations of the optoelectronic feedback loop allows to identify that the limited Q-factor of the blue fiber-based resonator bounds the noise reduction to a white frequency noise level close to 4×10^3 Hz^2/Hz. This noise reduction scheme could be, in a near future, applied to a single mode DFB GaN laser diode for further integration.

Appendix

In the following, we describe the complete derivation of S_Q (Eq. (6)) from cavity and PDH parameters. The response of the cavity, used as an optical reference, can be express as:

$$C(\nu) = \sqrt{1-\gamma}\frac{\sqrt{\kappa} - \sqrt{\kappa_c}\exp(-i\beta(\nu)L)}{1 - \sqrt{\kappa\kappa_c}\exp(-i\beta(\nu)L)} \tag{7}$$

where L is the cavity length and $\beta(\nu) = 2\pi\nu n/c$ the propagation constant (n is the refractive index of the fiber and c the speed of light in vacuum). γ corresponds to the optical losses, κ is the transmission coefficient of the optical coupler and κ_c represents the round trip loss of the ring.

The minimum of the cavity transmission, observed at the resonance frequencies, is given by:

$$T_{min} = (1-\gamma)\left(\frac{\sqrt{\kappa} - \sqrt{\kappa_c}}{1 - \sqrt{\kappa\kappa_c}}\right)^2 \tag{8}$$

and the maximum cavity transmission obtained between two resonances is:

$$T_{max} = (1-\gamma)\left(\frac{\sqrt{\kappa} + \sqrt{\kappa_c}}{1 + \sqrt{\kappa\kappa_c}}\right)^2 \tag{9}$$

For frequencies close to a resonance center ν_0 ($\nu \approx \nu_0$), $C(\nu)$ can be linearized as:

$$C(\nu) \approx \sqrt{T_{min}}[1 + ib(\nu - \nu_0)] \tag{10}$$

with:

$$b = \frac{(1-\kappa)\sqrt{\kappa_c}}{[\sqrt{\kappa} - \sqrt{\kappa_c}][1 - \sqrt{\kappa\kappa_c}]}\frac{2\pi}{\nu_{FSR}} \tag{11}$$

where $\nu_{FSR} = c/(nL)$ is the free spectral range of the ring cavity. The input laser field of optical frequency ν_L and amplitude M_0 is frequency modulated at the frequency F. For a small value of the modulation index β, the expression of the field is written by retaining only the terms of frequency ν_L, and $\nu_L \pm F$ in the Fourier development of $m(t)$:

$$m(t) = M_0[J_0(\beta)\exp(i2\,\pi\nu_L t) + J_1(\beta)\exp(i2\,\pi(\nu_L + F)t) + J_{-1}(\beta)\exp(i2\,\pi(\nu_L - F)t)] \tag{12}$$

where $J_i(.)$ is the i-order Bessel function. The cavity output field is thus of the form :

$$\begin{aligned} r(t) = M_0[&J_0(\beta)\exp(i2\,\pi\nu_L t)C(\nu_L) + J_1(\beta)\exp(i2\,\pi(\nu_L + F)t)C(\nu_L + F) \\ &- J_1(\beta)\exp(i2\,\pi(\nu_L - F)t)C(\nu_L - F)] \end{aligned} \tag{13}$$

in which we have made $J_{-1}(\beta) = -J_1(\beta)$. When the laser frequency is close to the resonance center ($\nu_L \approx \nu_0$), the amplitude response of the cavity, $C(\nu_L)$ can be given by Eq. (10). In the

Optics EXPRESS

PDH technique, the modulation frequency have to be greater than the resonance linewidth. This situation is shown on Fig. 5. Considering that this condition is fulfilled, which means that $C(\nu_L + F) \approx C(\nu_L - F) \approx \sqrt{T_{max}}$ (as shown in Fig. 5), the cavity output field can be expressed as:

$$r(t) = M_0[X + iY]\exp(i2\,\pi\nu_L t) \tag{14}$$

with $X = \sqrt{T_{min}}J_0(\beta)$ and $Y = b\sqrt{T_{min}}J_0(\beta)(\nu_L - \nu_0) + 2\sqrt{T_{max}}J_1(\beta)sin(\pi Ft)$.

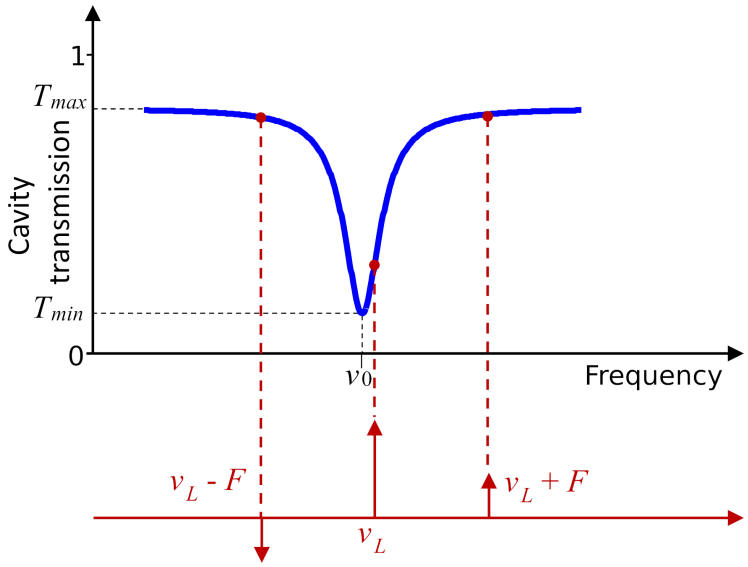

Fig. 5. In the PDH technique, when the laser frequency ν_L is close to the resonance center ν_0, the sidebands do not experience any attenuation or phase shift.

The photodiode generates a photocurrent proportional to r^*r of the form $i(t) = Kr^*(t)r(t)$ leading to the output signal of the photodetector:

$$V(t) = KZ_rM_0^2(X^2 + Y^2) + Z_rn(t) \tag{15}$$

where Z_r is the transimpedance gain and $n(t)$ represents the noise of the photocurrent. The output signal expressed by Eq. (15) can be rewritten as:

$$V(t) = V_0 + V_1(2\,\pi Ft) + V_2\cos(4\,\pi Ft) + Z_rn(t) \tag{16}$$

with the following voltage component expressions:

$$\begin{aligned} V_0 &= KZ_rM_0^2[T_{min}J_0^2(\beta) + b^2T_{min}J_0^2(\beta)(\nu_L - \nu_0)^2 + 2\,T_{max}J_1^2(\beta)] \\ V_1 &= 4\,KZ_rM_0^2b\sqrt{T_{min}T_{max}}J_0(\beta)J_1(\beta)(\nu_L - \nu_0) \\ V_2 &= -2\,KZ_rM_0^2T_{max}J_1(\beta)^2 \end{aligned} \tag{17}$$

The signal component at F detected by the lock-in amplifier at the cavity output, is proportional to the frequency detuning $x = K_2(\nu_L - \nu_0)$ where the frequency discriminator coefficient is expressed as:

$$K_2 = 2\,L_0KZ_rM_0^2b\sqrt{T_{min}T_{max}}J_0(\beta)J_1(\beta) \tag{18}$$

with L_0 is the gain of the lock-in amplifier.

Optics EXPRESS

Considering that the shot noise is the main contribution to the photocurrent noise, the unilateral power spectral density (PSD) of the photocurrent noise $n(t)$ is given by $S_n = 2qI_P$ where I_P is the mean photocurrent. When the laser frequency is locked onto the center of the resonance ($\nu_L = \nu_0$), the mean photocurrent is expressed as:

$$I_p = KM_0^2[T_{min}J_0^2(\beta) + 2\ T_{max}J_1^2(\beta)] \tag{19}$$

In the bandwidth of the lock-in amplifier, the unilateral PSD of the detected noise is found to be $S_{N_{dis}} = (L_0 Z_R)^2 qI_P$ which can be expressed as a frequency noise in $\mathrm{Hz}^2/\mathrm{Hz}$ as:

$$S_Q = \left(\frac{L_0 Z_R}{K_2}\right)^2 qI_p \tag{20}$$

Using Eqs. (18) and (19), one finds:

$$S_Q = \frac{q}{4\ KM_0^2 b^2}\left[\frac{1}{T_{max}J_1^2} + \frac{2}{T_{min}J_0^2}\right] \tag{21}$$

In the following we reformulate the Eq. (20) in terms of measurable quantities. Noting that $KM_0^2 = SP$ where S is the photodetector sensitivity and P the input power of the cavity, and introducing the FWHM of the resonance deduced from a Lorentzian approximation of the line shape $\Delta\nu = \frac{\nu_{FSR}(1-\sqrt{\kappa\kappa_c})}{\pi}$, the equivalent frequency noise of the discriminator can be rewritten as :

$$S_Q = \frac{q\Delta\nu^2}{16\ SPB^2}\left[\frac{1}{T_{max}J_1^2} + \frac{2}{T_{min}J_0^2}\right] \tag{22}$$

With $B = \frac{(1-\kappa)\sqrt{\kappa_c}}{\sqrt{\kappa}-\sqrt{\kappa_c}}$. The experimental measurement of the transmission coefficient κ and the round trip loss of the cavity κ_c give $B^2 = 5.4$ in our study which leads to the Eq. (6) given in the manuscript.

Funding. Labex Cluster of Excellence FIRST-TF (ANR-10-LABX-48-01); within the Program "Investissements d'Avenir" operated by the French National Research Agency (ANR) Agence Nationale de la Recherche project COMBO (18-CE24-0003-01).

Disclosures. The authors declare no conflicts of interest.

Data availability. Data underlying the results presented in this paper are not publicly available at this time but may be obtained from the authors upon reasonable request.

References

1. W.-C. Wang, H.-Y. Wang, and G.-R. Lin, "Ultrahigh-speed violet laser diode based free-space optical communication beyond 25 Gbit/s," Sci. Rep. **8**(1), 13142 (2018).
2. K. Nakamura, I. Mizukoshi, and M. Hanawa, "Optical wireless transmission of 405 nm, 145 Gbit/s optical IM/DD-OFDM signals through a 48 m underwater channel," Opt. Express **23**(2), 1558 (2015).
3. T.-C. Wu, Y.-C. Chi, H.-Y. Wang, C.-T. Tsai, and G.-R. Lin, "Blue laser diode enables underwater communication at 12.4 Gbps," Sci. Rep. **7**(1), 40480 (2017).
4. H. Leinen, D. Glässner, H. Metcalf, R. Wynands, D. Haubrich, and D. Meschede, "GaN blue diode lasers: a spectroscopist's view," Appl. Phys. B: Lasers Opt. **70**(4), 567–571 (2000).
5. I. Courtillot, J. Morville, V. Motto-Ros, and D. Romanini, "Sub-ppb NO_2 detection by optical feedback cavity-enhanced absorption spectroscopy with a blue diode laser," Appl. Phys. B **85**(2-3), 407–412 (2006).
6. X. Zeng, "Perspectives of active atomic clock based on modelocked semiconductor laser with rubidium vapor cell saturable absorber," Ph.D. thesis, Swiss Federal Institute of Technology in Lausanne (2015).
7. D. Hucul, J. E. Christensen, E. R. Hudson, and W. C. Campbell, "Spectroscopy of a synthetic trapped ion qubit," Phys. Rev. Lett. **119**(10), 100501 (2017).
8. B. Pasquiou, A. Bayerle, S. M. Tzanova, S. Stellmer, J. Szczepkowski, M. Parigger, R. Grimm, and F. Schreck, "Quantum degenerate mixtures of strontium and rubidium atoms," Phys. Rev. A **88**(2), 023601 (2013).

Optics EXPRESS

9. S. Stellmer, B. Pasquiou, R. Grimm, and F. Schreck, "Laser cooling to quantum degeneracy," Phys. Rev. Lett. **110**(26), 263003 (2013).
10. D. Pan, B. Arora, Y.-m. Yu, B. K. Sahoo, and J. Chen, "Optical-lattice-based Cs active clock with a continual superradiant lasing signal," Phys. Rev. A **102**(4), 041101 (2020).
11. X. Zang, T. Zhang, and J. Chen, "Magic wavelengths for a lattice trapped rubidium four-level active optical clock," Chin. Phys. Lett. **29**(9), 090601 (2012).
12. F. Favre, D. le Guen, J. Simon, and B. Landousies, "External-cavity semiconductor laser with 15 nm continuous tuning range," Electron. Lett. **22**(15), 795–796 (1986).
13. R. Maulini, "Broadly tunable mid-infrared quantum cascade lasers for spectroscopic applications," Ph.D. thesis, Université de Neuchatel (2006).
14. M. Horstjann, V. Nenakhov, and J. P. Burrows, "Frequency stabilization of blue extended cavity diode lasers by external cavity optical feedback," Appl. Phys. B **106**(2), 261–266 (2012).
15. X. Zeng, D. L. Boíko, G. Cosendey, M. Glauser, J.-F. Carlin, and N. Grandjean, "In-depth analysis of injection-seeded long external cavity InGaN/GaN surface-emitting laser," J. Appl. Phys. **113**(4), 043108 (2013).
16. X. Zeng and D. L. Boíko, "1/f noise in external-cavity InGaN diode laser at 420 nm wavelength for atomic spectroscopy," Opt. Lett. **39**(6), 1685–1688 (2014).
17. V. Maurice, Z. L. Newman, S. Dickerson, M. Rivers, J. Hsiao, P. Greene, M. Mescher, J. Kitching, M. T. Hummon, and C. Johnson, "Miniaturized optical frequency reference for next-generation portable optical clocks," Opt. Express **28**(17), 24708–24720 (2020).
18. T. Slight, S. Stanczyk, S. Watson, A. Yadav, S. Grzanka, E. Rafailov, P. Perlin, S. Najda, M. Leszczynski, S. Gwyn, and A. Kelly, "Continuous-wave operation of (Al, In)GaN distributed-feedback laser diodes with high-order notched gratings," Appl. Phys. Express **11**(11), 112701 (2018).
19. J. H. Kang, H. Wenzel, E. Freier, V. Hoffmann, O. Brox, J. Fricke, L. Sulmoni, M. Matalla, C. Stölmacker, M. Kneissl, M. Weyers, and S. Einfeldt, "Continuous-wave operation of DFB laser diodes based on gan using $10^{t}h$ -order laterally coupled surface gratings," Opt. Lett. **45**(4), 935–938 (2020).
20. T. Slight, A. Yadav, O. Odedina, W. Meredith, K. Docherty, E. Rafailov, and A. Kelly, "InGaN/GaN laser diodes with high order notched gratings," IEEE Photonics Technol. Lett. **29**(23), 2020–2022 (2017).
21. A. Congar, M. Gay, G. Perin, D. Mammez, J.-C. Simon, P. Besnard, J. Rouvillain, T. Georges, L. Lablonde, T. Robin, and S. Trebaol, "Narrow linewidth near-uv InGaN laser diode based on external cavity fiber bragg grating," Opt. Lett. **46**(5), 1077–1080 (2021).
22. G. Galzerano, E. Fasci, A. Castrillo, N. Coluccelli, L. Gianfrani, and P. Laporta, "Absolute frequency stabilization of an extended-cavity diode laser against doppler-free $H_2{}^{17}O$ absorption lines at 1384 μm," Opt. Lett. **34**(20), 3107–3109 (2009).
23. J. Morville, S. Kassi, M. Chenevier, and D. Romanini, "Fast, low-noise, mode-by-mode, cavity-enhanced absorption spectroscopy by diode-laser self-locking," Appl. Phys. B **80**(8), 1027–1038 (2005).
24. A. C. Ramdane, P. Grüning, V. Roncin, and F. Du-Burck, "Stability transfer at 1.5 μm for metrological applications using a commercial optical cavity," Appl. Opt. **56**(1), 8–14 (2017).
25. F. Kéfélian, H. Jiang, P. Lemonde, and G. Santarelli, "Ultralow-frequency-noise stabilization of a laser by locking to an optical fiber-delay line," Opt. Lett. **34**(7), 914 (2009).
26. O. Llopis, Z. Abdallah, V. Auroux, and A. Fernandez, "High spectral purity laser characterization with a self-heterodyne frequency discriminator," In *Proceedings of the 2015 IEEE International Frequency Control Symposium and European Frequency and Time Forum (joint conferences)* (IEEE, 2015), 602–605.
27. I. Outumuro, J. L. Valencia, J. Diz-Bugarin, I. Estevez-Caride, J. Blanco, and B. V. Dorrío, "Stabilization and calibration of an ECDL system with a Michelson interferometer," Proc. SPIE **8785**, 87855E (2015).
28. B. Merkel, D. Repp, and A. Reiserer, "Laser stabilization to a cryogenic fiber ring resonator," Opt. Lett. **46**(2), 444–447 (2021).
29. P. Grüning, A. Chaouche-Ramdane, K. Manamanni, T. Aoudjit, V. Roncin, and F. Du-Burck, "All-fiber ring-cavity for frequency stability transfer at 1.55 μm," Appl. Opt. **58**(6), 1502–1507 (2019).
30. P.-H. Merrer, O. Llopis, and G. Cibiel, "Laser Stabilization on a Fiber Ring Resonator and Application to RF Filtering," IEEE Photonics Technol. Lett. **20**(16), 1399–1401 (2008).
31. J. I. Kim, C. Y. Park, J. Y. Yeom, E. B. Kim, and T. H. Yoon, "Frequency-stabilized high-power violet laser diode with an ytterbium hollow-cathode lamp," Opt. Lett. **28**(4), 245–247 (2003).
32. P. Chang, S. Zhang, H. Shang, and J. Chen, "Stabilizing diode laser to 1 Hz-level allan deviation with atomic spectroscopy for Rb four-level active optical frequency standard," Appl. Phys. B **125**(11), 196 (2019).
33. O. Llopis, P. H. Merrer, H. Brahimi, K. Saleh, and P. Lacroix, "Phase noise measurement of a narrow linewidth cw laser using delay line approaches," Opt. Lett. **36**(14), 2713–2715 (2011).
34. G. D. Domenico, S. Schilt, and P. Thomann, "Simple approach to the relation between laser frequency noise and laser line shape," Appl. Opt. **49**(25), 4801–4807 (2010).
35. R. Drever, J. Hall, F. Kowalski, J. Hough, G. Ford, A. Munley, and H. Ward, "Laser phase and frequency stabilization using an optical resonator," Appl. Phys. B **31**(2), 97–105 (1983).
36. A. Novak, L. Simon, and P. Lotton, "Synchronized Swept-Sine: Theory, Application, and Implementation," J. Audio Eng. Soc. **63**(10), 786–798 (2015).

Optics EXPRESS

37. G. Bailly, O. Llopis, and A. Fernandez, "High spectral purity optical source stabilized on a fiber ring resonator," IEEE Photonics Technol. Lett. **32**(5), 255–258 (2020).